

Unified reference frame dq model of the brushless doubly fed machine

J. Poza[†], E. Oyarbide^{††}, D. Roye[‡] and M. Rodriguez[†]

[†] Faculty of Engineering, University of Mondragon, Loramendi 4, Aptdo. 23, 20500 Mondragón, Spain
e-mail: jgalarza@eps.mondragon.edu

^{††} Aragón Institute for Engineering Research (I3A), University of Zaragoza, María de Luna 1, 50018 Zaragoza, Spain,
e-mail: eoyarbid@unizar.es

[‡] Laboratoire d'Electrotechnique de Grenoble INPG/UJF-CNRS UMR 5529

Abstract: Control of the Brushless Doubly Fed Machine (BDFM) based on traditional multiple reference frames is complex. To simplify the control scheme, a new and simpler derivation of the dq model of the BDFM is proposed, leading to a unified-reference-frame model. This way, a simple dq model can be established, which could be an interesting tool for control-synthesis tasks. In order to determine the unified reference dq model, restrictions related to BDFM operation, as well as the exact rotor-cage configuration, have been considered. The proposed model has been validated by several experimental results. This work could facilitate future research on improved BDFM field-oriented control strategies.

List of symbols

p_1 (p_2)	number of pole pairs of the first (second) stator winding
n	number of rotor nests
θ_r	mechanical rotor-shaft displacement
δ	initial mechanical rotor-shaft angular position
γ	mechanical angular displacement of stator winding 2
θ_a	unified-reference-frame position in a p_1 -type pole-pair distribution
ω_r	rotor's mechanical angular speed
ω_a	angular speed of the unified reference frame
v_{s1} (v_{s2})	stator-winding 1 (2) fed voltage vector
i_{s1} (i_{s2})	stator-winding 1 (2) current vector
Ψ_{s1} (Ψ_{s2})	stator-winding 1 (2) flux linkage vector
i_{ri}	current of nest i of the rotor
i_r	rotor's equivalent current vector
Ψ_r	rotor flux-linkage vector
T_{em}	electromagnetic torque
R_{s1} (R_{s2})	stator-winding 1 (2) resistance
R_r	rotor resistance
L_{s1} (L_{s2})	stator-winding 1 (2) self inductance
L_r	rotor self inductance
L_{m1} (L_{m2})	inductance between the phase a of the stator winding 1 (2) and the reference loop of the rotor
L_{h1} (L_{h2})	unified frame stator-winding 1 (2) to rotor coupling inductance
K	arbitrary transformation ratio
V_c	control-winding phase voltage (RMS)
<i>Subscripts</i>	
$s1, s2, r$	stator winding 1, stator winding 2, rotor

p, c	power winding, control winding
<i>Superscripts</i>	
$\alpha\beta_1$	stator winding-1 reference frame in a p_1 -type pole-pair distribution
$\alpha\beta_2$	stator winding-2 reference frame in a p_2 -type pole-pair distribution
$\alpha\beta r_1$	rotor reference frame in a p_1 -type pole-pair distribution
$\alpha\beta r_2$	rotor reference frame in a p_2 -type pole-pair distribution
dq	arbitrary reference frame in a p_1 -type pole-pair distribution
p_1 (p_2)	p_1 -type (p_2 -type) winding distribution

1 Introduction

Recent developments have revitalised research activities in the area of doubly-fed machines [1], [2]. The expression doubly-fed applies, generally, to machines where electrical power can be fed or extracted from two accessible three-phase windings. The wound rotor induction machine is a good example. Generally the stator winding (through which most of the power flows) is connected directly to the grid and the rotor winding is connected to a bi-directional power converter. The power rating of the rotor winding, i.e. the converter size, depends on the required speed range and the reactive-power requirements. This fact can be of particular interest in systems with limited speed ranges, such as variable-speed wind turbines. The main problem is that the slip rings and wound-rotor arrangement render the rotor of a slip-ring doubly fed machine more vulnerable to faults than a cage induction machine. Among other

solutions, the use of the so-called brushless doubly fed machine (BDFM) could overcome this problem.

The BDFM (which is also known as a self-cascaded machine) is composed of two three-phase windings in the stator (called power winding, PW, and control winding, CW) and a special rotor winding [3]. Thanks to the specific design of the BDFM, the control winding can modify and control the rotor current which is being induced by the power winding. This is achieved by an electromagnetic cross-coupling effect between the two stator windings through the rotor. The existence of multiple reference frames, related to the two stator windings and the rotor, makes it difficult to exploit the well known standard induction-machine control strategies.

Wallace *et al.* developed the dynamic vector model of the BDFM referred to the rotor's shaft position [4], later validated in an experimental set-up [5]. The derivation of the model was carried out by orthogonal transformation matrices for a given machine configuration (a six-pole power winding, a two-pole control winding and a rotor with four nests). In [6] the same group generalised their previous work for an arbitrary pole number, and experimentally validated the developed steady-state model. Next, a BDFM model was derived assuming that the machine was composed of two superposed subsystems [7]-[8]. Each subsystem contained the dynamics of one of the two stator windings (PW or CW) and the corresponding rotor dynamics. The set of equations of the PW or CW subsystem were written in two different synchronous reference frames related to each pole-pair distribution. This leads to a couple of equations describing the dynamics of two independent rotor currents which correspond to two different synchronous reference frames. The electromagnetic torque depends on the current and the flux of both subsystems, as well as the so-called 'synchronous angle' between the two reference frames. Based on the control of this synchronous angle [8], a CW-rotor flux-oriented torque-control algorithm was developed.

Later on, a complete analysis of the synchronous steady-state operation of the BDFM was presented by Williamson *et al.* [9]. This work developed a generalised harmonic analysis of the BDFM, obtaining an accurate mathematical model. The resulting model was validated experimentally and iron losses and saturation effects were also investigated [10]. Note that, if sinusoidally distributed windings are considered, the BDFM model developed in [9] is equivalent to the steady-state version of the vector model presented in [4]. One of the main advantages of the generalised harmonic analysis approach is that it makes it possible to compute several interesting operating parameters, i.e. impedances, current densities and induction values. This work, together to the analysis methodology developed by the same authors in [11], [12] and [13], is a powerful tool for the study of the BDFM, which is especially useful for static-performance analysis as well as for machine-design tasks. Unfortunately, as it does not reflect the transient behaviour of the machine, the model can not be used for control purposes.

Muñoz and Lipo proposed dynamic complex vector models for both the cage induction machine [14] and the dual-stator-winding induction machine [15]. These models are based on complex vector notation, leading to a

complete but compact machine description, including transients. The generalised analysis method of [14] employed in the study of a dual-stator machine in [15], can also be applied to the study of the dynamics of any other doubly fed machine, such as the BDFM. Based on this approach, the authors proposed in [16] a unified-reference-frame vector model for the BDFM. Detailed description can be found in [17]. The model developed in [16] is mathematically equivalent to that presented in [7], but it is written in a unified reference frame, in contrast to the two reference frames required in [7]. Thanks to its simplicity, the unified-reference-vector model could be more convenient for control purposes. A vector control of the BDFM based on this model has been already proposed [18]. In this proposal, the generic reference frame is aligned with the PW flux vector. Experimental results presented in the same paper validate the approach and show that the model is well adapted for control synthesis tasks.

Later on, [19] proposes a generalised 'synchronous reference frame' model, which has been derived in a different way but becomes identical to the unified-reference-frame model of [16]. The unified-reference model has also been employed to investigate the open-loop stability of the BDFM, [17], [19] and [20].

This paper improves the derivation proposed in [16], eliminating some unnecessary steps. Simulated and experimental results validate the retained approach.

2 Coupling conditions

The coupled magnetic theory and complex space-vector notation will be used throughout the derivation [14]. The following general assumptions are made:

- (a) negligible saturation,
- (b) uniform air gap, and
- (c) sinusoidally distributed stator windings.

One of the three-phase windings of the stator is directly linked to the power line and it is usually denoted as the power winding (PW). It has a p_1 pole-pair distribution and most of the power flows through it. The additional three-phase winding of the stator is branched to a power converter. Its goal is to modify the electromagnetic state of the rotor windings, and so it is denoted as the control winding (CW). It has a p_2 pole-pair distribution. The BDFM must be designed carefully in such a way that:

- (i) The rotor-PW system behaves as a classical induction machine, i.e. a p_1 distribution-type current is induced in the rotor.
- (ii) The CW cannot directly influence any of the PW variables. This restriction can easily be fulfilled if $p_1 \neq p_2$ (in a practical BDFM design, other considerations must be taken into account in order to avoid the direct transformer coupling between the two stator windings).
- (iii) In order to control the machine, i.e. the electromagnetic state of the rotor, variables related to the CW must be able to modify the rotor current. Taking into account the p_1 -type distribution of the original rotor current related to the PW, the p_2 -type distribution of the CW and the fact that $p_1 \neq p_2$, the rotor must be designed in such a

way that a p_1 -type rotor current causes a p_2 -type rotor current (and vice versa). This way, if a p_1 -type rotor current exists, the same current also exists in a p_2 -type rotor distribution (and vice versa).

This last condition is the so-called indirect-cross-coupling condition. In fact, both the CW and the PW are coupled through the rotor. Next, we will show the special rotor configuration which fulfils this condition. The following relation expresses a generic space-vector representation of a variable x in a n -phase system:

$$\bar{x} \equiv \frac{2}{n} (x_1 + x_2 e^{j p \alpha_2} + x_3 e^{j p \alpha_3} + \dots + x_n e^{j p \alpha_n}) \quad (1)$$

where $2/n$ is the amplitude conservation factor, p is the number of the space harmonic and α_i is the mechanical angle between coil i and coil 1. Take an n -loop rotor whose current components 'exist' along a p_1 pole-pair distribution. These rotor currents can be represented by the next space vector related to the rotor reference:

$$\bar{i}_r^{p_1} = \frac{2}{n} (i_{r1} + i_{r2} b^{p_1} + i_{r3} b^{2p_1} + \dots + i_{rn} b^{p_1(n-1)}) \quad (2)$$

with $b = \exp(j2\pi/n)$. Individual loop currents can easily be obtained projecting this vector on each individual coil.

$$i_{ri} = \Re e \left\{ \bar{i}_r^{p_1} b^{-p_1(i-1)} \right\} = \frac{1}{2} \left(\bar{i}_r^{p_1} b^{-p_1(i-1)} + \bar{i}_r^{*p_1} b^{p_1(i-1)} \right) \quad (3)$$

In order to obtain a cross-coupling effect, $\bar{i}_r^{p_1}$ must also 'exist' or 'be visible' along a p_2 pole-pair distribution, getting a nonzero $\bar{i}_r^{p_2}$. Computing $\bar{i}_r^{p_2}$

$$\bar{i}_r^{p_2} = \frac{2}{n} (i_{r1} + i_{r2} b^{p_2} + i_{r3} b^{2p_2} + \dots + i_{rn} b^{p_2(n-1)}) \quad (4)$$

and replacing (3) in (4) we obtain

$$\bar{i}_r^{p_2} = \frac{1}{n} \left[\bar{i}_r^{p_1} \left\{ 1 + b^{(p_2-p_1)} + \dots + b^{(n-1)(p_2-p_1)} \right\} + \bar{i}_r^{*p_1} \left\{ 1 + b^{(p_2+p_1)} + \dots + b^{(n-1)(p_2+p_1)} \right\} \right] \quad (5)$$

A nonzero $\bar{i}_r^{p_2}$ is obtained if at least one of the two terms of the right-hand side are nonzero, leading to two possible configurations, see Appendix (Section 8.1):

Configuration 1:

$$\frac{(p_2 - p_1)}{n} = q \quad (6)$$

$$\bar{i}_r^{p_2} = \bar{i}_r^{p_1} \quad (7)$$

with $q = 0, \pm 1, \pm 2, \dots$

Configuration 2:

$$\frac{(p_2 + p_1)}{n} = q \quad (8)$$

$$\bar{i}_r^{p_2} = \bar{i}_r^{*p_1} \quad (9)$$

In the first configuration, the rotor current has exactly the same value in the two possible distributions, whereas in the second configuration one of the current vectors behaves as the conjugate of the other. According to these relations it becomes straightforward to change from a p_1 -type reference frame to a p_2 -type one or vice versa, the key step of the derivation presented in this paper.

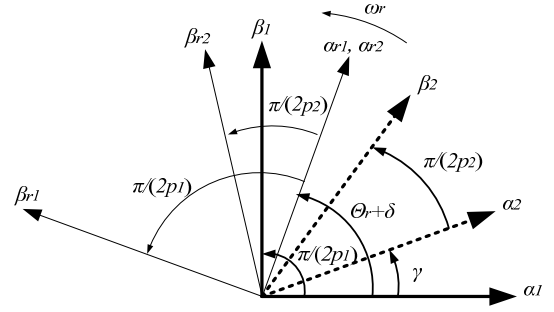


Fig. 1 Initial reference frames (mechanical angles)

3 Unified Reference Frame Model of the BDFM

It is assumed that the stator has two sinusoidally distributed windings with different number of poles ($p_1 \neq p_2$). The rotor of the BDFM is configured with n symmetrical nests in such a way that the second condition (9) is fulfilled, being $p_2 + p_1 = n$. Although each nest can be built of several isolated loops, one unique loop per nest will be initially considered.

3.1 Initial multiple-reference-frame model of the BDFM

There are three initial reference frames (shown in Fig. 1):

(a) PW reference $\alpha\beta_1$ related to a p_1 pole-pair-type distribution, which is used as the overall static reference frame.

(b) CW reference $\alpha\beta_2$ related to a p_2 pole-pair-type distribution and located at a mechanical angular position of γ radians from $\alpha\beta_1$.

(c) Rotor references $\alpha\beta_{r1}$ and $\alpha\beta_{r2}$ related, respectively, to a p_1 and p_2 pole-pair-type distributions which are located at a mechanical angular position of $\theta_r + \delta$ from $\alpha\beta_1$ (being δ the initial position).

Computing the flux space vectors, the voltage equations can easily be defined in these multiple reference frames as follows [14], [15]:

$$\mathbf{v}_{s1}^{\alpha\beta_1} = R_{s1} \bar{i}_{s1}^{\alpha\beta_1} + \frac{d\bar{\Psi}_{s1}^{\alpha\beta_1}}{dt} \quad (10)$$

$$\bar{\Psi}_{s1}^{\alpha\beta_1} = L_{s1} \bar{i}_{s1}^{\alpha\beta_1} + K \frac{n}{2} L_{m1} e^{jp_1(\theta_r + \delta)} \bar{i}_r^{\alpha\beta_{r1}} \quad (11)$$

$$\mathbf{v}_{s2}^{\alpha\beta_2} = R_{s2} \bar{i}_{s2}^{\alpha\beta_2} + \frac{d\bar{\Psi}_{s2}^{\alpha\beta_2}}{dt} \quad (12)$$

$$\bar{\Psi}_{s2}^{\alpha\beta_2} = L_{s2} \bar{i}_{s2}^{\alpha\beta_2} + K \frac{n}{2} L_{m2} e^{jp_2(\theta_r + \delta - \gamma)} \bar{i}_r^{\alpha\beta_{r2}} \quad (13)$$

$$\mathbf{v}_r^{\alpha\beta_{r1}} = R_r \bar{i}_r^{\alpha\beta_{r1}} + \frac{d\bar{\Psi}_r^{\alpha\beta_{r1}}}{dt} \quad (14)$$

$$\begin{aligned}\bar{\Psi}_r^{\alpha\beta n} &= L_r \bar{i}_r^{\alpha\beta n} + \frac{3}{2} \frac{L_{m1}}{K} e^{-jp_1(\theta_r + \delta)} \bar{i}_{s1}^{\alpha\beta_1} \\ &+ \frac{3}{2} \frac{L_{m2}}{K} e^{jp_1(\theta_r + \delta - \gamma)} \bar{i}_{s2}^{\alpha\beta_2}\end{aligned}\quad (15)$$

where

$$\bar{i}_r^{\alpha\beta r_1} \equiv \frac{1}{K} \frac{2}{n} (i_{r1} + i_{r2} b^{p_1} + \dots + i_{rn} b^{p_1(n-1)}) \quad (16)$$

$$\bar{i}_r^{\alpha\beta r_2} \equiv \frac{1}{K} \frac{2}{n} (i_{r1} + i_{r2} b^{p_2} + \dots + i_{rn} b^{p_2(n-1)}) \quad (17)$$

In the previous model, K is an arbitrary gain that modifies the amplitude of the rotor-vectors. For $K=1$, the amplitude of the resulting rotor current vector will be equal to the maximum phase value. On the other hand, to obtain the same equivalent mutual inductance from rotor to stator as from stator to rotor, the following constraint must be fulfilled:

$$K \frac{n}{2} L_{m1} = \frac{3}{2} \frac{L_{m1}}{K} \quad (18)$$

obtaining

$$K = \sqrt{\frac{3}{n}} \quad (19)$$

Taking the value obtained for (19), we obtain the initial multiple-reference model:

$$\mathbf{v}_{s1}^{\alpha\beta_1} = R_{s1} \bar{i}_{s1}^{\alpha\beta_1} + \frac{d\Psi_{s1}^{\alpha\beta_1}}{dt} \quad (20)$$

$$\Psi_{s1}^{\alpha\beta_1} = L_{s1} \bar{i}_{s1}^{\alpha\beta_1} + L_{h1} e^{jp_1(\theta_r + \delta)} \bar{i}_r^{\alpha\beta r_1} \quad (21)$$

$$\mathbf{v}_{s2}^{\alpha\beta_2} = R_{s2} \bar{i}_{s2}^{\alpha\beta_2} + \frac{d\Psi_{s2}^{\alpha\beta_2}}{dt} \quad (22)$$

$$\Psi_{s2}^{\alpha\beta_2} = L_{s2} \bar{i}_{s2}^{\alpha\beta_2} + L_{h2} e^{jp_2(\theta_r + \delta - \gamma)} \bar{i}_r^{\alpha\beta r_2} \quad (23)$$

$$\mathbf{v}_r^{\alpha\beta r_1} = R_r \bar{i}_r^{\alpha\beta r_1} + \frac{d\Psi_r^{\alpha\beta r_1}}{dt} \quad (24)$$

$$\begin{aligned}\bar{\Psi}_r^{\alpha\beta r_1} &= L_r \bar{i}_r^{\alpha\beta r_1} + L_{h1} e^{-jp_1(\theta_r + \delta)} \bar{i}_{s1}^{\alpha\beta_1} \\ &+ L_{h2} e^{jp_1(\theta_r + \delta - \gamma)} \bar{i}_{s2}^{\alpha\beta_2}\end{aligned}\quad (25)$$

with

$$L_{h1} = \frac{\sqrt{3n}}{2} L_{m1}, \quad L_{h2} = \frac{\sqrt{3n}}{2} L_{m2} \quad (26)$$

3.2 Unified dq -reference-frame model

As it can be observed, the initial set of (20)-(25) is referred to three different frames and two possible pole-pair distributions are considered. The goal is to get a set of equations with a unified reference frame with a given pole-pair distribution p (e.g. p_1) located at an arbitrary mechanical position (θ_a/p_1) from $\alpha\beta_1$. This is easily achieved if next steps are followed (for more details see Appendix, Section 8.2). First, the transformation relation between the $\alpha\beta_2$ - p_2 and $\alpha\beta_1$ - p_1 systems is developed. It is assumed that the rotor of the BDFM fulfils the second coupling condition (9). Next, we can define a generic dq reference frame with a p_1 pole-pair-type distribution and

located at any given mechanical position θ_a/p_1 from $\alpha\beta_1$. Vector transformations from original reference frames to generic dq reference frame are obtained. Finally, by means of these vector transformations, the machine model (20)-(25) is expressed in a common dq generic reference frame (27)-(32) (dq -reference symbols have been removed to simplify resulting expressions).

$$\mathbf{v}_{s1} = R_{s1} \bar{i}_{s1} + \frac{d\Psi_{s1}}{dt} + j\omega_a \Psi_{s1} \quad (27)$$

$$\bar{\Psi}_{s1} = L_{s1} \bar{i}_{s1} + L_{h1} \bar{i}_r \quad (28)$$

$$\mathbf{v}_{s2} = R_{s2} \bar{i}_{s2} + \frac{d\Psi_{s2}}{dt} + j[\omega_a - \omega_r(p_1 + p_2)] \Psi_{s2} \quad (29)$$

$$\Psi_{s2} = L_{s2} \bar{i}_{s2} + L_{h2} \bar{i}_r \quad (30)$$

$$\mathbf{v}_r = R_r \bar{i}_r + \frac{d\Psi_r}{dt} + j(\omega_a - p_1 \omega_r) \Psi_r \quad (31)$$

$$\Psi_r = L_r \bar{i}_r + L_{h1} \bar{i}_{s1} + L_{h2} \bar{i}_{s2} \quad (32)$$

This model is similar to the well known vector model of a standard induction machine. The expressions related to stator winding 1 are the same. In rotor flux equation, the influence of the two stator currents is represented. In stator winding 2, the factor $\omega_a - (p_1 + p_2)\omega_r$ represents the relative angular velocity between the reference frames dq and $\alpha\beta_2$.

The electromagnetic torque can be expressed as:

$$T_{em1} = \frac{3}{2} p_1 \text{Im} \left[\bar{\Psi}_{s1}^* \bar{i}_{s1} \right] \quad (33)$$

$$T_{em2} = \frac{3}{2} p_2 \text{Im} \left[\bar{\Psi}_{s2}^* \bar{i}_{s2} \right] \quad (34)$$

$$T_{em} = T_{em1} + T_{em2} \quad (35)$$

For a rotor with multiple loop nests, a similar derivation can be carried out. See Appendix, Section 8.3 for a model of a BDFM with multiple loop nested rotor.

4 Experimental verification

To validate the proposed model, simulations and experimental tests have been carried out. Matlab-Simulink software has been used for simulations. Experimental results have been obtained by means of a BDFM prototype fed by two independent voltage sources.

4.1 PW-flux-reference-frame machine model

The selected dq reference frame is aligned with the PW-flux orientation, $\Psi_{dp} = |\Psi_p|$ and $\Psi_{qp} = 0$. From equations (27)-(32), we obtain the final unified dq reference model (we have removed vector notation to simplify the resulting expressions):

$$\mathbf{v}_p = R_{sp} \mathbf{i}_p + \frac{d\Psi_p}{dt} + j\omega_p \Psi_p \quad (36)$$

$$\Psi_p = L_{sp} \mathbf{i}_p + L_{hp} \mathbf{i}_r \quad (37)$$

$$\mathbf{v}_c = R_{sc} \mathbf{i}_c + \frac{d\Psi_c}{dt} + j(\omega_p - (p_p + p_c)\omega_r) \Psi_c \quad (38)$$

$$\Psi_c = L_{sc} \mathbf{i}_c + L_{hc} \mathbf{i}_r \quad (39)$$

$$\mathbf{v}_r = R_r \mathbf{i}_r + \frac{d\Psi_r}{dt} + j(\omega_p - p_p \omega_r) \Psi_r \quad (40)$$

$$\Psi_r = L_r i_r + L_{hc} i_c + L_{hp} i_p \quad (41)$$

$$T_{em} = \frac{3}{2} p_p \text{Im} \left[\Psi_p^* i_p \right] + \frac{3}{2} p_c \text{Im} \left[\Psi_c^* i_c \right] \quad (42)$$

4.2 Experimental test bench

The goal of the BDFM prototype is to collect the maximum experimental data needed in the validation of the theoretical models and the control strategies, regardless of the optimization of machine performance. The power ratings of the two stator windings are the same (220V/50Hz, 10A), in such a way that two different PW and CW configurations can be tested by the same machine. One of the windings (the PW in our tests) has two poles and the other (the CW for us) is composed of six poles. The rotor is formed of four nests, with a single loop per nest (slots for additional two loops per nest are available). There are two different ways of measuring the rotor current in the laboratory. One of them employs a current transducer placed at the rotor which is coupled to a wireless communication system [21], [22]. In our case, the laboratory prototype has been equipped with a slip-rings brush system, which conducts the rotor current to a static environment, where the rotor winding is short-circuited. As the high current and small voltage values of the cast-rotor configuration makes this last solution unfeasible, copper-wire-type coils have been employed. This way, the current involved decreases and the brush-slip-ring contact-voltage drop becomes negligible compared with resulting higher rotor voltages. Though the final BDFM is not optimal in performance, it is suitable for experimental validation of models and control strategies.

Figure 2 shows a section of the BDFM prototype. It is built around the core of an IEC-180 frame four-pole wound rotor induction machine. The core is 200mm long and the stator is composed of 36 slots, with a 180mm inner diameter. The two stator windings have 23 turns per coil with a 2.075mm² wire and each rotor coil is made up of 65 turns of a 1.77mm² wire (rated for 10A RMS). The airgap is 0.6mm wide. For further constructional details, see [17].

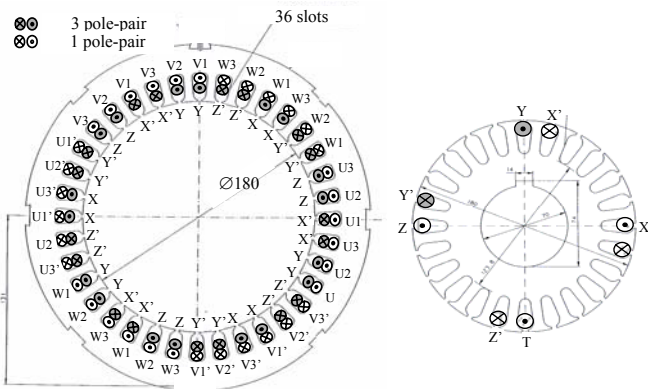


Fig. 2 Constructional details of the BDFM prototype

If stable operation is assured, the BDFM could operate from standstill to $2 \times \omega_{syn}$. The BDFM shows large unstable domains under open-loop operation, so in this work only subsynchronous speeds are considered. Saturation problems are avoided by a conservative design of the magnetic circuit. It is designed in such a way that the rated

CW flux could be reached along all the operating range. At nominal excitation level, the RMS value of the flux density in the airgap is $B_{sp} \approx 0.122T$ RMS for the PW and $B_{sc} \approx 0.433T$ RMS for the CW case. Steady-state results of this prototype are available in [17] and [23].

Relevant parameters employed for simulation tasks are collected in Table 1. Rotor resistance is directly measured through the available external terminals. L_{sp} and L_{sc} are calculated at a no-load test of single fed operation. In these tests the ‘effective-airgap’ curves related to each stator winding are obtained ([23]). L_{hp} , L_{hc} and L_r are computed taking into account these ‘effective-airgap’ curves. These inductances depend on the magnetic excitation level. In this work, the PW flux linkage is nearly constant and the CW flux linkage varies from 0.42 to 0.56 Wb RMS. Constant parameters have been considered, computed at $|\Psi_p| = 0.7Wb$ RMS and $|\Psi_c| = 0.5Wb$ RMS, which correspond to the RMS values of the airgap flux densities $B_{sp} \approx 0.152T$ RMS and $B_{sc} \approx 0.322T$ RMS.

Table 1: BDFM electrical parameters for simulation

	PW	CW	Rotor
Resistance (Ω)	$R_{sp}=1.732$	$R_{sc}=1.079$	$R_r=0.473$
Self Inductance (mH)	$L_{sp}=714.8$	$L_{sc}=121.7$	$L_r=132.6$
Mutual Inductance (mH)	$L_{hp}=242.1$	$L_{hc}=59.8$	

The experimental test bench is located at the Power Electronics Laboratory of the University of Mondragón (Fig. 3). The BDFM is on the left, coupled to a controlled reversible DC motor (on the right), which emulates the mechanical behaviour of the load. An additional wound-rotor induction machine related to other research activities is also coupled to the same shaft. To minimise any nonmodelled electromagnetic coupling, it is desirable to feed the CW with an ideal nonmodulated continuous voltage source. This is possible by means of a synchronous generator driven by a variable-speed induction-motor system (on the right-bottom corner of Fig. 3). The speed of the induction motor fixes the CW-feed frequency and the excitation of the synchronous generator fixes the CW-voltage level. The PW is directly connected to the standard European 400V-50Hz grid.

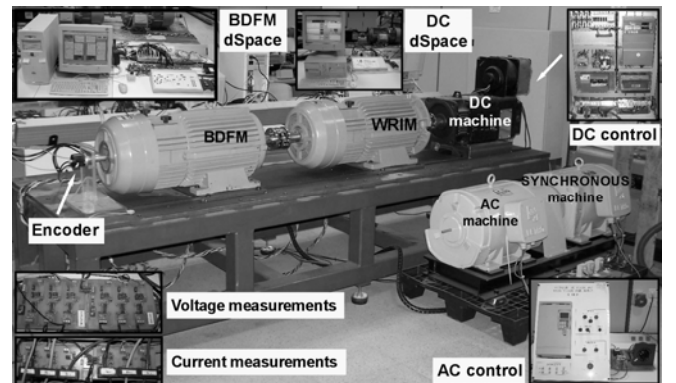


Fig. 3 Test setup

A DSP-based dSpace DS 1102 platform provides the speed/torque reference to the DC regulator. The measurement equipment is composed by an incremental

optical encoder and two three-phase voltage/current sensors (voltage measurement based on ISO 122 insulation amplifiers and current sensors based on LEM LA55/p transducers). These signals are captured and processed by an additional DSP-based dSpace DS1103 platform.

4.3. Comparison of simulated and experimental results

The proposed unified-reference-frame model is based on the knowledge of the PW flux position, which is obtained by means of a voltage-model-based estimator. This type of estimator integrates the electromotive force; thus some corrections have to be made to avoid the integration of DC offsets and to overcome the initial conditions problem. The estimation algorithm implemented in this paper uses a modified integrator based on the control of the quadrature of the $\alpha\beta$ flux components ([24], Algorithm 3: modified integrator with adaptive compensation). Owing to the quasiconstant amplitude and frequency of the PW flux, accurate estimation is achieved without difficulty. The resulting flux components are used in (43) to compute the electromagnetic torque produced by the PW:

$$T_{emp} = \frac{3}{2} p_p (\Psi_{ap} i_{\beta p} - \Psi_{\beta p} i_{ap}) \quad (43)$$

The same strategy developed for the PW case is used for flux and torque estimation in the CW case.

Data are captured at a sample time of $h=100\mu s$ and logged in a file. Comparison variables are obtained from experimental data by off-line algorithms and compared with simulation results. The simulation step is very small (quasicontinuous simulation), being experimental data interpolated at each step. Figure 4 depicts the comparison schema employed to validate the proposed unified dq reference model. The dq model receives dq voltage and rotor-speed data and outputs dq -current and electromagnetic-torque values. Experimental three-phase currents are converted to the unified dq reference frame.

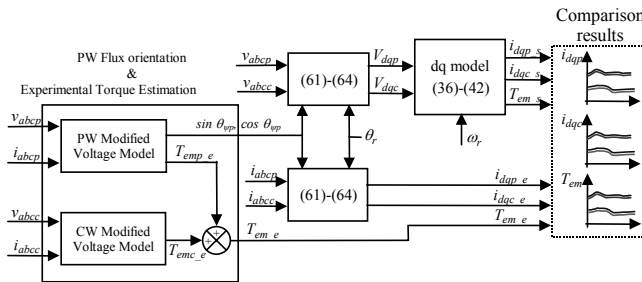


Fig. 4 Comparison schema of theoretical and experimental behaviour

In the experiments, the BDFM is always in an open-loop synchronous operation mode, so CW-current amplitude must be high enough to ensure adequate magnetisation (static synchronous condition) and rotor speed must be within the stable operation range (dynamic synchronous condition) [20]. The synchronous operation speed is equal to

$$\omega_r = \frac{\omega_p + \omega_c}{p_p + p_c} \quad (44)$$

where ω_p and ω_c are the electrical angular velocities of the PW and CW voltages, respectively. These angular speeds can take positive or negative values, depending on the phase sequence of the two feedings. Usually, a positive angular velocity is considered for the line-fed PW, so there are two operation cases: the subsynchronous case, where ω_c takes negative values; and the supersynchronous case, where ω_c takes positive values.

In open-loop control, this BDFM prototype shows a narrow stable domain in supersynchronous operation. Scalar current control or vector control schemes render the system stable at any speed range, but they are not feasible if a synchronous generator feeds the CW. Because of that, only the subsynchronous zone is explored in these tests.

Any variation in the voltage fed or in the load torque produces damped oscillations of the BDFM variables (currents, torque, speed etc.). After a short description of the steady state, the load-torque-variation case will be studied.

4.3.1 Steady-state current waveforms: In this Section experimentally obtained and simulated waveforms of the stator currents are compared. The BDFM is operating at $V_p=230V$ RMS, $f_p=50Hz$, $V_c=29V$ RMS, $f_c=11Hz$ and $\omega_r=61.2$ rad/s. No load torque is applied by the DC motor. Figure 5 compares simulated and experimental CW phase current. As can be observed, the model gives an accurate prediction of systems behaviour. The main difference is a high-order harmonic in the experimental current. The frequency of this harmonic, for any rotor speed, is three times the frequency of the PW current, and it could be caused by any nonmodelled nonlinear characteristic.

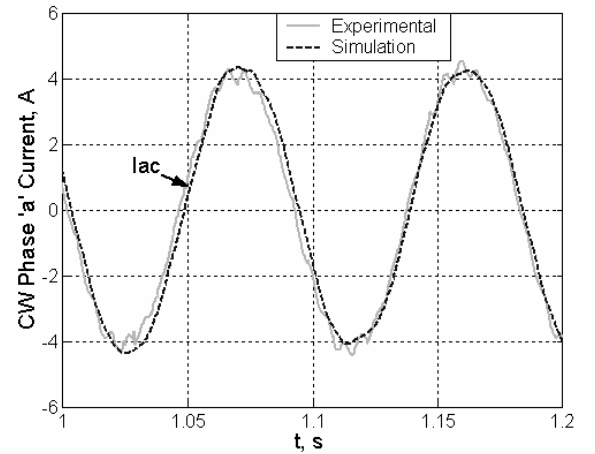


Fig. 5 One-phase current of the CW

Figure 6 shows the PW-current evolution. In the experimental case, a small subharmonic located at around 11Hz can be identified. Although it seems to be a direct CW-to-PW-coupling case, if several tests are carried out considering different speed values, the related frequency becomes that of the maximum common subharmonic of both PW and CW feed frequencies. Although the source of these oscillations must be investigated further, their relative low amplitude can be neglected for control purposes and their study falls in the field of BDFM optimization, which is outside the scope of the paper.

4.3.2 Load torque perturbation: In this experiment, steady-state synchronous operation is perturbed by a load-torque variation. As speed is related to CW frequency ($f_p=50\text{Hz}$, $f_c=14.24\text{Hz}$, $\omega_r=56.16\text{ rad/s}$), and provided that stable operation is assured [20], electromagnetic torque evolves towards the new load requirement whereas shaft speed oscillates around the steady-state synchronous operation speed.

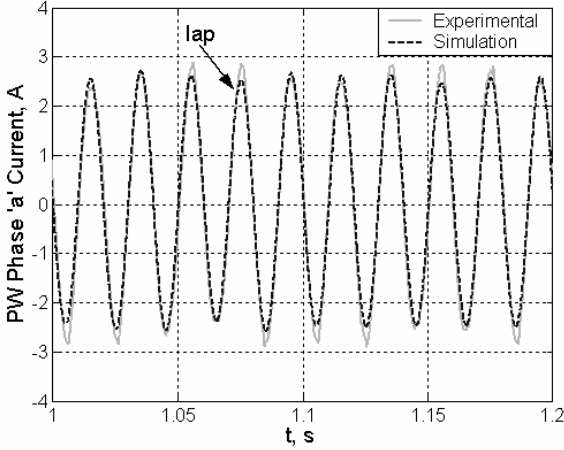


Fig. 6 One-phase current of the PW

Figure 7 shows the above-mentioned speed oscillations during the transient. As the CW current increases from a no-load state to a load state, an important voltage drop is caused by the output impedance of the synchronous generator.

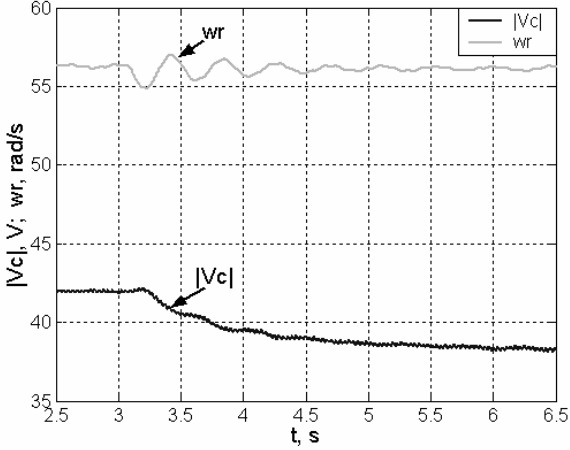


Fig. 7 Rotor speed and V_c (RMS)

Figure 8 shows dq -current components. Good matching is observed between experimental and simulated values. Any torque variation must modify quadrature current values (Fig. 8b) and must nearly hold direct-current values. However in Fig. 8a a nonnegligible direct current variation is observed. These variations are due to the cross-coupling effect of quadrature currents in the CW-voltage equation. As CW-voltage amplitude is maintained nearly constant, quadrature-current variations imply changes in direct-current value.

Figure 9 shows the torque step applied by the DC machine and the corresponding electromagnetic response of the BDFM. A constant offset of average value 5.3Nm is

observed. This torque-offset value deserves some clarification. The test bench consists of three machines sharing a common shaft, all of them equipped by several slip-ring brush systems. In addition, both the wound-rotor induction machine and the BDFM are cooled by self-ventilation systems. Overall brush-ring contact friction and aerodynamic losses are the source of observed high torque levels, which have been approximately modelled as:

$$T_{mech} = k_v \omega_r + k_f \quad (45)$$

with $k_v = 0.012\text{ Nms/rad}$ and $k_f = 4.62\text{ Nm}$. These values have been estimated through DC-motor-based tests and justify the observed torque offset.

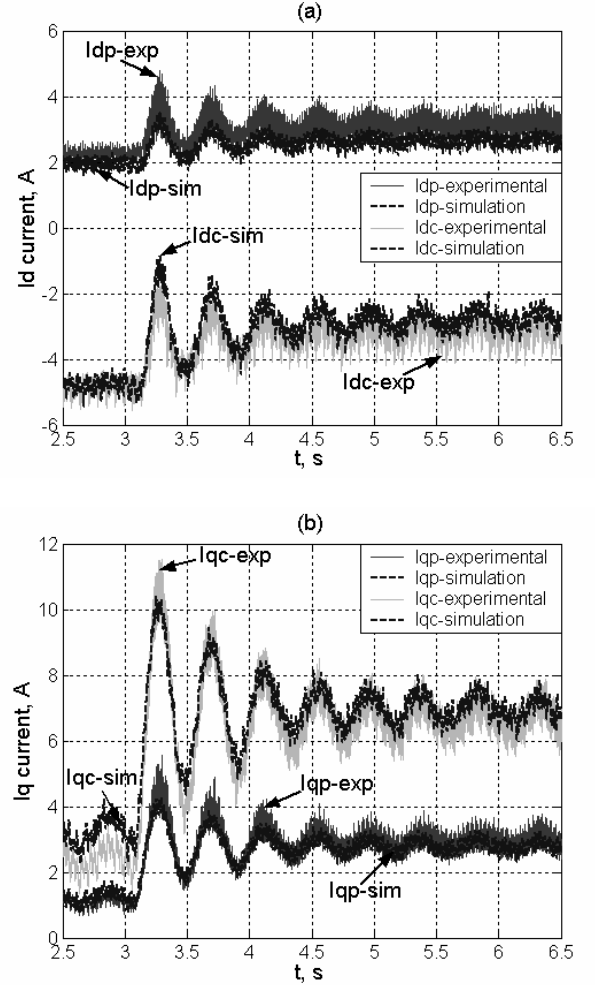


Fig. 8 Stator i_d, i_q currents

According to the experimental results, the proposed unified reference dq model offers an accurate prediction of the dynamic behaviour of the BDFM. If an advanced control algorithm has to be designed, a good dynamic model becomes crucial. On the other hand, constant deviations of dq current values can easily be compensated by any control system. These deviations can be originated by erroneous parameter estimations or parameter deviations, as well as by nonmodelled iron losses, which have to be included in the model if efficiency has to be computed.

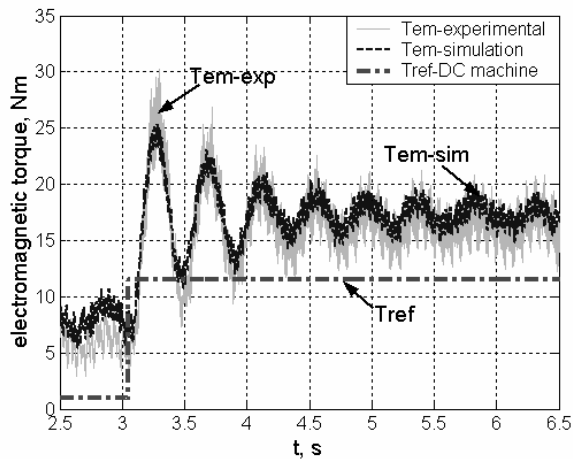


Fig. 9 Electromagnetic torque

Some extra harmonic components appear in phase experimental currents, but the resulting high-frequency variable oscillations in the dq reference-frame can easily be rejected by the control system.

5 Conclusions

In this paper, a new derivation of the unified-reference-frame dq model of the BDFM has been presented. Experimental results have validated the theoretical development. The proposed derivation exploits the complex vector notation and leads to a simple derivation of the unified- dq -reference-frame model.

The unified-reference-frame model of the BDFM has the same structure as the well known vector models of standard induction machines. This is an important issue because it allows advantage to be taken of the set of control techniques and analysis tools that have previously been developed for other machines, especially for the cage induction machine and the wound-rotor induction machine. In this way, the authors are already working on scalar and vector control schemes based on the proposed unified- dq -reference-frame model of the BDFM. Results will be addressed soon.

6 Acknowledgements

This work has been partially supported by the Basque Country Government (PI 2003-11) and by the Spanish Ministry of Education and Science (ENE2005-09218-C2-01/ALT).

7 References

[1] Hopfensperger, B., and Atkinson, D.J.: "Doubly-fed a.c. machines: classification and comparison". *EPE 2001-Graz*, DS 3.4-2.
 [2] Hopfensperger, B., and Atkinson, D.J. Lakin R.A.: "Combined magnetising flux oriented control of the cascaded doubly-fed induction machine". *IEE Proc. Electr. Power Appl.*, 2001, Vol. 148, No. 4, pp. 354-362.
 [3] Roberts, P.C., McMahon, R.A., Tavner, P.J., Maciejowski, J.M., and Flack, T.J.: "Equivalent circuit for the brushless doubly fed machine (BDFM) including parameter estimation

and experimental verification", *IEE Proc.-Electr. Power Appl.*, 2005, Vol. 152, No. 4, pp. 933-942.
 [4] Li, R., Wallace, A.K., and Spée, R.: "Two-axis model development of cage-rotor brushless doubly-fed machines". *IEEE Transactions on Energy Conversion*, 1991, Vol. 6, pp. 453-460.
 [5] Li, R., Wallace, A., and Spee, R.: "Dynamic Simulation of Brushless Doubly-Fed Machines", *IEEE Transactions on Energy Conversion*, 1991, Vol. 6, No. 3, pp. 445-452.
 [6] Boger, M.S., Wallace, A.K., Spée, R., and Li, R.: "General Pole Number Model of the Brushless Doubly-Fed Machine", *IEEE Transactions on Industry Applications*, 1995, Vol. 31, No. 5, pp. 1022-1995.
 [7] Zhou, D., Spée, R., and Alexander, G.C.: "Experimental Evaluation of a Rotor Flux Oriented Control Algorithm for Brushless Doubly-Fed Machines", *IEEE Transactions of Power Electronics*, 1997, Vol. 12, No. 1, pp. 72-78.
 [8] Zhou, D., and Spée, R.: "Synchronous frame model and decoupled control development for doubly-fed machines", *IEEE PESC Conf.*, 1994, pp. 1129-1236.
 [9] Williamson, S., Ferreira, A.C., and Wallace, A.K.: "Generalized theory of the brushless doubly-fed machine. Part 1: Analysis". *IEE Proc. Electr. Power Appl.*, 1997, Vol. 144, No. 2, pp. 111-122.
 [10] Williamson, S., and Ferreira, A.C.: "Generalized theory of the brushless doubly-fed machine. Part 2: Model verification and performance". *IEE Proc. Electr. Power Appl.*, 1997, Vol. 144, No. 2, pp. 123-129.
 [11] Williamson, S., and Smith, A.C.: "Field analysis for rotating induction machines and its relationship to the equivalent-circuit method", *IEE Proc. Pt. B*, 1980, Vol. 127, No. 2, pp. 83-90.
 [12] Williamson, S.: "Power-factor improvement in cage-rotor induction motors", *IEE Proc. Pt. B*, 1983, Vol. 130, No. 2, pp. 121-129.
 [13] Williamson, S., and Laithwaite, E.R.: "Generalised harmonic analysis for the steady-state performance of sinusoidally-excited cage induction motors", *IEE Proc. Pt. B*, 1983, Vol. 132, No. 3, pp. 157-163.
 [14] Muñoz, A.R., and Lipo, T.A.: "Complex vector model of the squirrel-cage induction machine including instantaneous rotor bar currents". *IEEE Trans. on Ind. Appl.* 1999, Vol. 35, No. 6, pp. 1332-1340.
 [15] Muñoz, A.R., and Lipo, T.A.: "Dual stator winding induction machine drive". *IEEE Trans. on Ind. Appl.*, 2000, Vol. 36, No. 5, pp. 1369-1379.
 [16] Poza, J., Oyarbide, E., Foggia, A., and Roye, D.: "Complex Vector Model of the Brushless Doubly-Fed Machine" in *Proceedings of the 2002 SPEEDAM conference*, Juin 2002, Ravello (Italy), pp. B4.13-B4.18.
 [17] Poza, J.: "Modélisation, conception et commande d'une machine asynchrone sans balais doublement alimentée pour la génération à vitesse variable". PhD Thesis, Institut National Polytechnique de Grenoble & Mondragon Unibertsitatea, October 2003.
 [18] Poza, J., Oyarbide, E., and Roye, D.: "New Vector Control Algorithm for Brushless Doubly-Fed Machines". In *Proceedings of the 2002 IEEE IECON conference*, Seville (Spain), November 2002.
 [19] Roberts, P.C.: "A Study of Brushless Doubly-Fed (Induction) Machines", PhD. Thesis, University of Cambridge, September 2004 (revised January 2005).
 [20] Poza, J., Oyarbide, E., Roye, D., and Sarasola, I.: "Stability Analysis of a BDFM under Open-Loop Voltage Control". In *Proceedings of the 2005 EPE conference*, Dresden (Germany), September 2005.
 [21] Abdi-Jalebi, E. Roberts, P.C., and E, McMahon R.A.: "Real-time rotor bar current measurement using a rogowski coil transmitted using wireless technology". *18th Intl. Power*

Systems Conf. (PSC2003), Iran, Volume 5, pages 1-9, October 2003.

- [22] Roberts, P.C., Abdi-Jalebi, E., McMahon R.A., and Flac, T. J.: "Real-time rotor bar current measurements using bluetooth technology for a brushless doubly-fed machine (bdfm)". *IEE Int. Conf. Power Electronics, Machines and Drives*, Volume 1, pages 120-125., March 2004.
- [23] Poza, J., Foggia, A., Oyarbide, E., and Roye, D.: "Brushless Doubly-Fed Machine Model". In Proceedings of the International Conference on Electrical Machines, ICEM 2002, Brugges, Belgium.
- [24] Hu, J., and Wu, B.: "New Integration algorithms for estimating motor flux over a wide speed range". *IEEE Trans. on Power Electronics. Appl.*, September 1998, Vol. 13, No. 5, pp. 969-977.

8 Appendixes

8.1 Conditions for the cross coupling-effect

In (5), to obtain a non-zero $\bar{i}_r^{p_2}$ at least one of the two terms of the right hand side must be nonzero, so

$$\sum_{m=1}^n e^{j\frac{2\pi}{n}(m-1)(p_2-p_1)} \neq 0 \quad (46)$$

or

$$\sum_{m=1}^n e^{j\frac{2\pi}{n}(m-1)(p_2+p_1)} \neq 0 \quad (47)$$

These nonzero values are obtained when:

$$e^{j\frac{2\pi}{n}(m-1)(p_2-p_1)} = 1 \quad (48)$$

or

$$e^{j\frac{2\pi}{n}(m-1)(p_2+p_1)} = 1 \quad (49)$$

which can be assured if one of the following two conditions is fulfilled

$$\frac{(p_2 - p_1)}{n} = q \quad (50)$$

$$\frac{(p_2 + p_1)}{n} = q \quad (51)$$

with $q = 0, \pm 1, \pm 2, \dots$. In the first case we obtain

$$\sum_{m=1}^n e^{j\frac{2\pi}{n}(m-1)(p_2-p_1)} = n \quad (52)$$

$$\sum_{m=1}^n e^{j\frac{2\pi}{n}(m-1)(p_2+p_1)} = 0 \quad (53)$$

leading to a configuration where the rotor current has exactly the same value in the two distributions,

$$\bar{i}_r^{p_2} = \bar{i}_r^{p_1} \quad (54)$$

In the second case, we obtain

$$\sum_{m=1}^n e^{j\frac{2\pi}{n}(m-1)(p_2-p_1)} = 0 \quad (55)$$

$$\sum_{m=1}^n e^{j\frac{2\pi}{n}(m-1)(p_2+p_1)} = n \quad (56)$$

so one of the current vectors becomes the conjugate of the other:

$$\bar{i}_r^{p_2} = \bar{i}_r^{p_1*} \quad (57)$$

8.2 Transformations between different reference frames

8.2.1 Coupling relation $\bar{x}^{\alpha\beta_2} = f(\bar{x}^{\alpha\beta_1})$: It is assumed that the rotor of the BDFM fulfils the second coupling condition (9) and maximizes the number of nests, i.e., $p_1 + p_2 = n$, which implies that:

$$\bar{x}^{\alpha\beta r_2} = \bar{x}^{\alpha\beta r_1*} \quad (58)$$

It can be easily deduced that:

$$\bar{x}^{\alpha\beta_2} = e^{jp_2(\theta_r + \delta - \gamma)} \bar{x}^{\alpha\beta r_2} \quad (59)$$

$$\bar{x}^{\alpha\beta_1} = e^{jp_1(\theta_r + \delta)} \bar{x}^{\alpha\beta r_1} \quad (60)$$

Combining (58)-(60) we obtain

$$\bar{x}^{\alpha\beta_1} = e^{j\theta_g} \bar{x}^{\alpha\beta_2*} \quad (61)$$

with $\theta_g = (p_1 + p_2)(\theta_r + \delta) - p_2\gamma$. Thanks to these last relations, it is possible to express any motor variable in the fixed unique $\alpha\beta_1$ reference frame.

8.2.2 Vector transformations from original reference frames to generic dq reference frame:

We can define a generic dq reference frame with a p_1 pole-pair-type distribution and located at any given mechanical position θ_a/p_1 from $\alpha\beta_1$. The vector transformation involved is defined as

$$\bar{x}^{\alpha\beta_1} = e^{j\theta_a} \bar{x}^{dq} \quad (62)$$

Employing (58)-(62) it is straightforward to obtain the next relationships:

$$\bar{x}^{\alpha\beta_2} = e^{j(\theta_g - \theta_a)} \bar{x}^{dq*} \quad (63)$$

$$\bar{x}^{\alpha\beta r_1} = e^{j[\theta_a - p_1(\theta_r + \delta)]} \bar{x}^{dq} \quad (64)$$

$$\bar{x}^{\alpha\beta r_2} = e^{-j[\theta_a - p_1(\theta_r + \delta - \gamma)]} \bar{x}^{dq*} \quad (65)$$

In this way any machine variable can be defined in a generic dq reference frame.

8.3 Modelling in the case of a rotor with multiple loop nests

This configuration can be considered as a superposition of different rotor subsystems. Each subsystem groups all the loops at the same relative position in their nest [9]. Equations for the multiple-loop case are obtained in a same way than for a single-loop case. Only coupling impedances between different subsystems of the rotor must be added. The following equations represent the model of the BDFM

considering a generic number of rotor subsystems (or loops per nest), denoted as m .

$$\mathbf{v}_{s1} = R_{s1} \dot{\mathbf{i}}_{s1} + \frac{d\Psi_{s1}}{dt} + j\omega_a \Psi_{s1} \quad (66)$$

$$\Psi_{s1} = L_{s1} \dot{\mathbf{i}}_{s1} + \sum_{i=1}^m L_{h1m} \dot{\mathbf{i}}_{ir} \quad (67)$$

$$\mathbf{v}_{s2} = R_{s2} \dot{\mathbf{i}}_{s2} + \frac{d\Psi_{s2}}{dt} + j[\omega_a - \omega_r(p_1 + p_2)]\Psi_{s2} \quad (68)$$

$$\Psi_{s2} = L_{s2} \dot{\mathbf{i}}_{s2} + \sum_{i=1}^m L_{h2m} \dot{\mathbf{i}}_{ir} \quad (69)$$

$$\mathbf{v}_{ir} = R_r \dot{\mathbf{i}}_{ir} + \frac{d\Psi_{ir}}{dt} + j(\omega_a - p_1 \omega_r)\Psi_{ir} \quad (70)$$

$$\Psi_{ir} = \sum_{j=1}^m L_{rj} \dot{\mathbf{i}}_{jr} + L_{h1i} \dot{\mathbf{i}}_{s1} + L_{h2i} \dot{\mathbf{i}}_{s2} \quad (71)$$

$$T_{em1} = \frac{3}{2} p_1 \operatorname{Im} \left[\dot{\Psi}_{s1}^* \dot{\mathbf{i}}_{s1} \right] = \frac{3}{2} p_1 \sum_{i=1}^m \left\{ L_{h1i} \operatorname{Im} \left[\dot{\mathbf{i}}_{s1}^* \dot{\mathbf{i}}_{ir} \right] \right\} \quad (72)$$

$$T_{em2} = \frac{3}{2} p_2 \operatorname{Im} \left[\dot{\Psi}_{s2}^* \dot{\mathbf{i}}_{s2} \right] = \frac{3}{2} p_2 \sum_{i=1}^m \left\{ L_{h2i} \operatorname{Im} \left[\dot{\mathbf{i}}_{s2}^* \dot{\mathbf{i}}_{ir} \right] \right\} \quad (73)$$

$$T_{em} = T_{em1} + T_{em2} \quad (74)$$

By means of some approximate dynamic reductions, a simplified model can also be obtained [17].